Journal of Materials Chemistry A

Accepted Manuscript

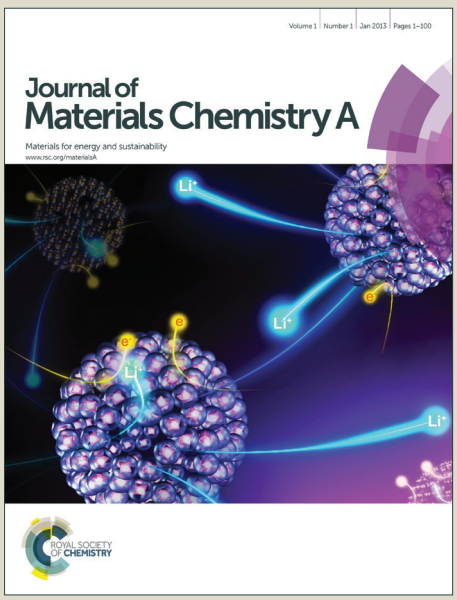

ROYAL SOCIETY OF CHEMISTRY

www.rsc.org/materialsA

Microstructure Design of Hybrid CoO@NiO and Graphene Nano-architectures for Flexible High Performance Supercapacitors

*By Zan Gao,† Ningning Song,† Xiaodong Li†,**

† Department of Mechanical and Aerospace Engineering, University of Virginia, 122 Engineer's Way, Charlottesville, VA 22904-4746 (USA)

∗ Corresponding author: *E-mail: xl3p@virginia.edu*

Abstract

We demonstrate rational design and fabrication of CoO nano-architectures with different morphologies (sheet-like, petal-like and urchin-like) on flexible activated carbon textiles (ACT) by simply changing the reactant concentration. We further unveiled that the electrochemical properties of CoO nanostructures are morphology-dependent. The specific capacitance increased exponentially with the surface/volume ratio of nanostructures. The architecture with higher surface area exhibits better electrochemical performance. Due to its higher surface/volume ratio and better electrochemical performance, urchin-like CoO nanostructure was further chosen as a backbone to deposit NiO nanoflakes to construct a hierarchical core/shell CoO@NiO hybrid nanostructure. Flexible ACTs wrapped with conductive graphene were used as negative material. After coated with PVA-KOH polymer gel which served as both the solid state electrolyte and separator, the flexible core/shell CoO@NiO/ACT//ACT/graphene asymmetric cell exhibited an exceptional combination of electrochemical properties in terms of working potential (1.6 V), energy density (52.26 Wh kg^{-1}), maxmium power density (9.53 KW kg^{-1}), and cycling stability (97.53% capacitance retention after 2000 cycles even under harsh working condition). Such hierarchical nanostructure on cotton-enabled flexible textile substrate should find more applications in next-generation flexible solid-state power sources for future wearable electronics.

Keywords: *Morphology Control; Metal Oxide; Graphene; Flexible; Supercapacitor*

1. Introduction

To solve the energy crisis in 21st century, tremendous efforts have been devoted to developing energy storage and conversion devices to meet the increasing demand for energy.[1,2] Batteries, fuel cells, and electrochemical capacitors, which directly convert chemical energy into electrical energy, have been proven effective for practical energy storage and conversion. Recently, electrochemical capacitors (ECs) (also known as supercapacitors or ultracapacitors) are emerging as very promising energy storage devices for flexible electronics and electric vehicles due to the excellent combination of their electrochemical properties such as high power density, good pulse charge-discharge performance, long lifespan, and low maintenance cost.[3,4] However, compared with lithium-ion batteries, supercapacitors often suffer from relatively low energy density, which limits their practical applications.[5] Progresses have been made in developing new electrode materials with high surface area architectures for enhancing the electrochemical performance of supercapacitors.[6-8] To date, various electrode materials including carbon materials,[9-12] transition-metal oxides and hydroxides,[13-17] conducting polymers[18-21] have been explored for supercapacitor applications.

It has been challenging to achieve joint improvements in all aspects of electrochemical properties and performance. For example, carbon materials have higher power density and longer lifespan, but lower capacitance and energy density. In contrast, transition metal oxides possess higher energy density but relatively lower power density and poorer cyclic life due to their intrinsic poor electrical conductivity and short diffusion distance (~20 nm), which limit the contribution of the inner active materials to the total capacitance.[22] The electrochemical performance of an electrode material depends strongly on the morphology and microstructure of the material.[23] An intelligent approach to push up the electrode material's performance is to create architectures with high specific surface area, which is anticipated to achieve a joint improvement in electrical conductivity, specific capacitance, energy density and power density, and cyclic stability.[24] The future of electronics will be flexible and wearable. Many attempts have been devoted to developing safe, lightweight and flexible power sources to meet the

urgent needs of flexible and wearable electronics.[25] However, to date, a streamlined manufacturing process for integrating flexible energy storage devices with wearable electronics has not realized. Most of the reported flexible electrodes were fabricated by depositing active materials on conductive carbon cloth, carbonized or paper-like polymers.[26-28] Textile-based energy devices with outstanding mechanical robustness and superior electrochemical performance are still lacking. It is challenging to fabricate nanoarchitectures with pre-designed morphologies and tunable functions on flexible textile substrates.

Recently, transition metal oxides have been widely investigated as pseudocapacitive or "battery-type" Faradic electrode materials due to their good electroactivity, high theoretical capacitance, low cost, and natural abundance.[29,30] However, the reported values are often much lower than theoretically predicted capacities. To enhance the specific capacitance, cycle life and rate performance of transition metal oxide electrodes, many efforts have been devoted to rationally design of hetero-/homo-nanostructures. Fan *et al.* reported that core/shell Co_3O_4@NiO hetero-nanostructure deposited on nickel foam showed a specific capacitance of 853 F g^{-1} at the current density of 2 A g^{-1}.[31] Zhang *et al.* demonstrated that the enhanced electrochemical performance of hierarchical Co_3O_4@$NiCo_2O_4$ nanoforest on Ni-foam (areal capacitance is 2.04 F cm^{-2} at the scan rate of 5 mV s^{-1}).[32] Recently, the fabricated $NiCo_2O_4$@$NiCo_2O_4$ homo-nanostructure on flexible activated carbon textile also exhibited exceptional electrochemical performance.[33] In those studies, the integrated hierarchical 3D porous structure, coupling two types of materials and/or nanostructures on conductive substrates, brings together many competitive advantages such as easy accessibility of electrolyte ions, rich electroactive sites, short ion diffusion path, superior current collection efficiency and the fascinating synergetic effects of different components. Among various transition metal oxides, Co_3O_4 and NiO have aroused great interests because of their high theoretical capacity (3560 F g^{-1} and 2584 F g^{-1}, respectively), good electronic conductivity, favorable capacitive characteristics and controllable size and morphology.[34] In fact, CoO possesses a higher theoretical capacitance of 4292 F g^{-1}, which can be a better candidate for

supercapacitor applications.[35] But till now, there are only fewer reports about the nanostructured CoO and its nanocomposites for supercapacitor applications.[36,37]

Energy density and power density of supercapacitor are always contradictory each other. Energy density can be enhanced at the sacrifice of power density by using pesudocapacitive transition metal oxides. To resolve such contradiction between energy density and power density, an intelligent approach is to develop an asymmetric supercapacitor, which consists of a battery-type Faradic electrode (as energy source) and a capacitor-type electrode (as power source).[38] Carbon is the most widely used capacitor-type electrode material with high power density and excellent rate performance due to its good electrical conductivity and often high surface area in its electrode architecture.[39] Among various carbon materials, two-dimensional (2D) single layered graphene has been regonized as an ideal candidate because of its high specific surface area, superior electrical conductivity, high flexibility, outstanding mechanical properties and relative wide operation windows.[40] Graphene-based films and papers with three dimensional (3D) porous structures have also been intensively explored for flexible supercapacitor applications.[41-44]

Cotton is flexible, green and renewable and is the most widely used natural fibers for soft and breathable clothing and textiles.[45] Our previous studies have shown that the activated carbon textile (ACT) converted from a cotton T-shirt can be an excellent wearable platform for flexible energy storage devices because of its lightweight, eminent flexibility, and excellent conductivity.[46] In this paper, we report a new route for fabricating hybrid CoO@NiO nano-architectures on ACT with high surface area. Battery-type Faradic CoO nanostructures with different morphologies (sheet-like, petal-like and urchin-like) were controllably synthesized on ACTs by simply changing the reactant concentration during the hydrothermal process. We unveiled that the electrochemical properties of CoO nanostructures are morphology-dependent. The specific capacitance increased exponentially with the surface/volume ratio of nanostructures. The architecture with higher surface area exhibits better electrochemical performance. Due to its higher surface/volume ratio and better electrochemical performance, urchin-like CoO was

further chosen as a backbone to deposit NiO nanoflakes to construct a hierarchical core/shell CoO@NiO hybrid nanostructure. The hybrid CoO@NiO nanostructured electrode with high surface area enables fast charge accumulation and ion transport. For the negative electrode, we coated ACT fibers with corrugated, high conductive graphene coating by a simple dipping, drying and reducing process. The graphene coating, serving as a current "expressway", bridged the electrolyte and current substrate, ensuring higher current collection efficiency and faster ion transition. Finally, the nanostructured core/shell CoO@NiO/ACT (severving as the positive electrode), ACT/graphene (serving as the negative electrode), and PVA-KOH gel (serving as both the solid state electrolyte and separator) were assembled into a flexible all-solid-state (CoO@NiO/ACT//ACT/graphene) asymmetric supercapacitor, which synergically worked together to achieve an exceptional combination of electrochemical properties in terms of working potential (1.6 V), energy density (52.26 Wh kg^{-1}), power density (9.53 KW kg^{-1}), and cycling stability (capacitance retention ratio of 97.53% after 2000 cycles).

2. Experiment Section

2.1 Preparation of Flexible CoO@NiO/ACT Positive Electrode

Fabrication of CoO nano-architectures on ACT with different morphologies

All chemicals were used after purchasing without further purification. A commercial cotton T-shirt was cleaned by distilled water in ultrasonic bath prior to activation. Activation of cotton T-shirt into ACT was performed following our previously established method.[33] CoO nano-architectures of different morphologies were grown on ACT fibers via a simple hydrothermal process. Typically, 0.01086 g of $Co(NO_3)_2 \cdot 6H_2O$, 0.0269 g NH_4F, and 0.1051 g of urea (the concentration of reactants is named as 1 C) were dissolved in 70 mL distilled water. The resulting solution was transferred into a 100 mL Teflon-lined stainless autoclave with a piece of vertically suspended ACT (1 cm × 2 cm) in the solution. Then, the autoclave was placed in an electric oven at 120 ℃ for 5 h. Finally, the as-prepared products were washed with ethanol and distilled water for several

times, dried at 80 ℃ overnight, and annealed at 450 °C in argon atmosphere for 2 h to produce CoO/ACT. To achieve different morphologies the reactant concentration was varied from 1 C to 10 C. Sheet-like, petal-like, and urchin-like CoO nanostructures were uniformly deposited on ACT fibers at the reactant concentration of 1 C, 5 C and 10 C, respectively.

Coating NiO nanoflakes onto urchin-like CoO nanowires

The screening on the as-synthesized CoO nanostructures showed that the urchin-like CoO nanostructure exhibited superior electrochemical performance. To further enhance its electrochemical properties NiO nanoflakes were deposited onto the urchin-like CoO nanostructure by a simple chemical bath deposition process, forming hierarchical core/shell CoO@NiO precursor.[47] Typically, 2 mL of aqueous ammonia (25-28%) was added to the mixture of 5 mL of 1 M nickel sulfate, and 8 mL of 0.25 M potassium persulfate to form a deposition solution. The obtained urchin-like CoO/ACT was vertically dipped in the above solution and kept for 10 min at room temperature. The obtained sample was rinsed with distilled water and then dried at 80 °C for 12 h. The as-prepared hybrid CoO@NiO precursor was further annealed at 450 ℃ under argon gas protection for 2 h to realize a flexible hierarchical core/shell CoO@NiO/ACT electrode.

2.2 Preparation of Flexible ACT/Graphene Negative Electrode

Graphite oxide was synthesized from natural graphite flakes by a modified Hummers method.[48] The obtained graphite oxide was further exfoliated by ultrasonication in an ultrasonic bath for 1 h to prepare graphene oxide. Then, the above graphene oxide solution was centrifuged at 3000 rpm for 5 min to remove aggregates, forming a brown graphene oxide aqueous colloid with a concentration of 4 mg mL^{-1}. A piece of ACT (1 cm × 2 cm) was then soaked with the clean graphene oxide aqueous colloid. After drying at 60 °C for 6 h, the as-prepared ACT with graphene oxide coating was carried out at 450 ℃ 1 h with

argon/hydrogen mixture gas (v/v 90/10) for the thermal reduction of ACT/graphene oxide to prepare a flexible ACT/graphene negative electrode.

2.3 Characterization Methods

The microstructure of the as-prepared samples was characterized by scanning electron microscopy (SEM; FEI Quanta 650) and transmission electron microscopy (TEM; JEOL 2000FX), high resolution transmission electron microscopy (HRTEM, FEI Titan) and atomic force microscopy (AFM; Nanoscope IIIa). The crystallographic structure of the synthesized materials was determined by a PANalytical X'Pert Pro Multi-Purpose Diffractometer (MPD) equipped with Cu K_α radiation (λ = 0.15406 nm). Raman measurements were carried out by a Renishaw InVia Raman microscope at 785 nm (with 5% Laser Power).

2.4 Fabrication and Electrochemical Characterization of Flexible, All-Solid-State Asymmetric Supercapacitors

The asymmetric supercapacitors presented in this paper were assembled with two pieces of flexible electrodes (positive and negative) face-to-face separated by the solid-state polymer gel electrolyte. The polymer gel electrolyte was prepared by mixing 3 g KOH and 6 g PVA in 60 mL deionized water at 80 ºC while being stirred magnetically until the solution became clear. Both the positive and negative electrodes were firstly dipped into the gel electrolyte solution for 3 min to soak gel electrolyte. After solidified at room temperature, two pieces of flexible electrodes separated by the PVA/KOH gel film were used to assemble a flexible asymmetric supercapacitor. The as-obtained solid-state polymer PVA/KOH gel film severed as both the separator and electrolyte. The electrochemical properties of the assembled flexible asymmetric supercapacitors were measured by using a CHI 660E electrochemical workstation. Cyclic voltammograms (CV), galvanostatic charge/discharge curves, and electrochemical impedance spectroscopy (EIS) in the frequency range from 100 kHz to 0.05 Hz with an AC

perturbation of 5 mV were used to evaluate the electrochemical performance of the flexible solid-state asymmetric supercapacitors.

3. Results and Discussion

3.1 Positive Electrode Materials

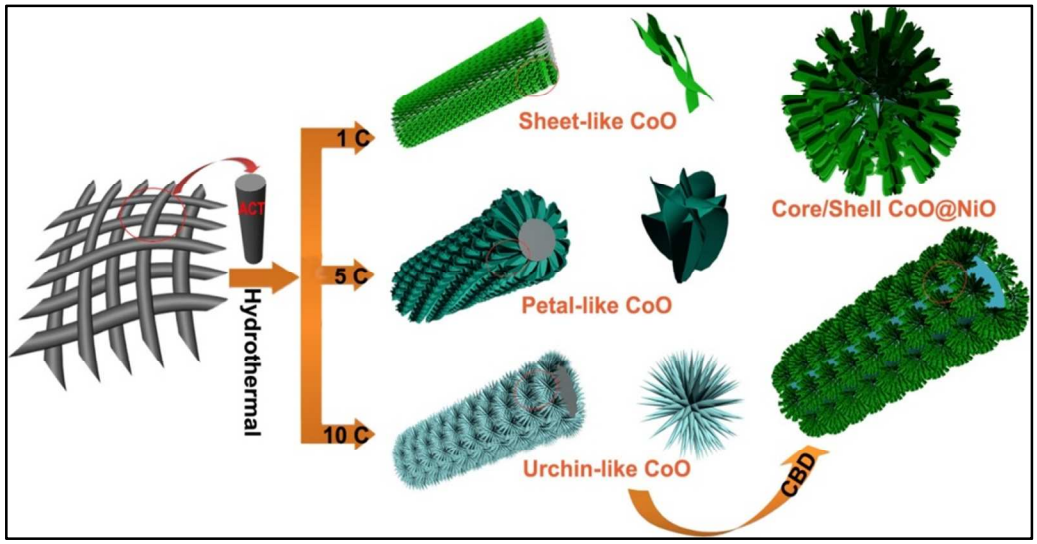

Figure 1 Schematic illustration of the formation processes of CoO nanostructures of different morphologies and the core/shell CoO@NiO nanocomposite on ACT.

The specific capacitances of transition metal oxides are usually sensitive to the thickness and mass of the active materials because of their poor conductivity.[49] An intelligent strategy to enhance electrochemical performance of transition metal oxides is to tune their microstructure to achieve large specific surface area. Figure 1 schematically illustrates the design and fabrication procedure of CoO nano-architectures of different morphologies on ACT fibers. The morphologies of CoO were found to be dependent strongly on the reactant concentration. Sheet-like, petal-like and urchin-like CoO nano-architectures were uniformly anchored on individual ACT fibers at the reactant concentration of 1 C, 5 C and 10 C, respectively. Microporous transition metal oxide nanowires often possess higher conductivity and more active for energy storage applications. Therefore, the hydrothermally synthesized urchin-like CoO nanoarrays were chosen as the backbone (core) for the deposition of NiO nanoflakes (shell) by a simple chemical bath deposition method. Finally, a hierarchical core/shell CoO@NiO

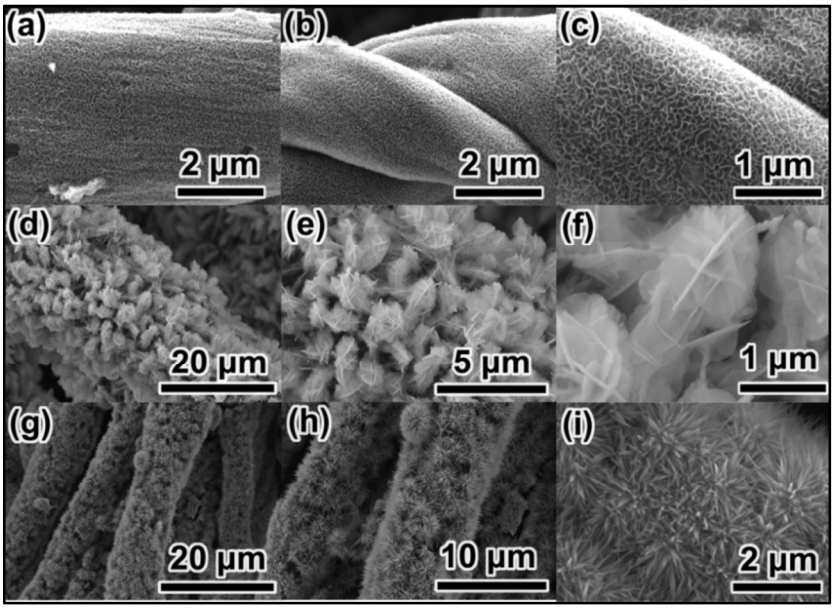

Figure 2 (a-c) SEM images of sheet-like CoO on ACT fibers at different magnifications; (d-f) SEM images of petal-like CoO on ACT fibers at different magnifications; (g-h) SEM images of urchin-like CoO on ACT fibers at different magnifications.

heterogeneous nanostructure with plenty of interspaces was closely anchored on the ACT fibers, which can be directly used as the binder-free flexible electrode. Importantly, the absence of conductive agent and polymer binders could effectively avoid the "dead volume" of active materials during the energy storage procedure. Such unique 3D hierarchical nanostructure not only enhances the contact between active material and substrate, but also shorts the ion transport path and facilitates the continuous charge transfer, jointly improving the electrochemical performance.

Three different types of CoO nanostructures grown on ACT fibers were prepared by coupled hydrothermal and annealing processes. The morphologies and microstructure of CoO nano-architectures on ACT fibers are shown in Figure 2. As shown in Figures 2a-c, at the relatively low reactant concentration of 1 C, ACT fibers were uniformly covered by vertically grown CoO nanoarrays with cross-linked porous structure. Upon increasing reactant concentration up to 5 C, petal-like CoO nanosheets were assembled together to form flower-like nanotrees, closely anchored on the surfaces of ACT (Figures 2d-f). Those hierarchical nanotrees were uniformly distributed on individual ACT fibers to form a thick nanoforest, which provides larger surface areas for ion attachment, improving electrochemical performance. Interestingly, when the reactant concentration

was increased up to 10 C, urchin-like CoO nanospheres with interconnected CoO nanowires were jointly grown on ACT fibers to form open porous nanojungles with plenty of interspaces (Figures 2g-i). Such special nano-architecture possesses higher surface/volume ratio and reaction activity, thereby enhancing its electrochemical performance. The chemical reactions involved in the hydrothermal synthesis and post annealing process can be expressed with the following equations:[50,51]

$$Co^{2+} + F^- \rightarrow CoF^+ \quad (1)$$

$$Co(NH_2)_2 + H_2O \rightarrow NH_3 + CO_2 \quad (2)$$

$$CO_2 + H_2O \rightarrow HCO_3^- + H^+ \quad (3)$$

$$HCO_3^- \rightarrow CO_3^{2-} + H^+ \quad (4)$$

$$NH_3 \cdot H_2O \rightarrow NH_4^+ + OH^- \quad (5)$$

$$CoF^+ + 0.5CO_3^{2-} + OH^- + 0.11H_2O \rightarrow Co(CO_3)_{0.5}(OH) \cdot 0.11H_2O + F^- \quad (6)$$

$$2Co(CO_3)_{0.5}(OH) \cdot 0.11H_2O \xrightarrow{Ar} 2CoO + 1.22H_2O + CO_2 \quad (7)$$

The morphological change with the reactant concentration can be explained by the interplays of the nucleation rate, the growth rate of nucleus and Ostwald-Ripening mechanism.[52] From the viewpoint of nucleation rate, the lager reactant concentration should result in a higher nucleation rate. Thus, much more nuclei formed in the solution at high reactant concentration. At the relatively low reactant concentration, a small amount of CoO precursor nuclei first formed on the surface of ACT, and grew slowly, leading to CoO precursor nanosheets vertically grown on ACT. With further increasing reactant concentration, a large number of nuclei formed at the initial stage, the growth of nuclei and the aggregation of particles were both promoted. According to the Ostwald-Ripening mechanism,[53] small particles were absorbed by the relatively large ones, therefore a higher density of urchin-like CoO precursor nanoshpheres was synthesized at the high reactant concentration during the hydrothermal process.

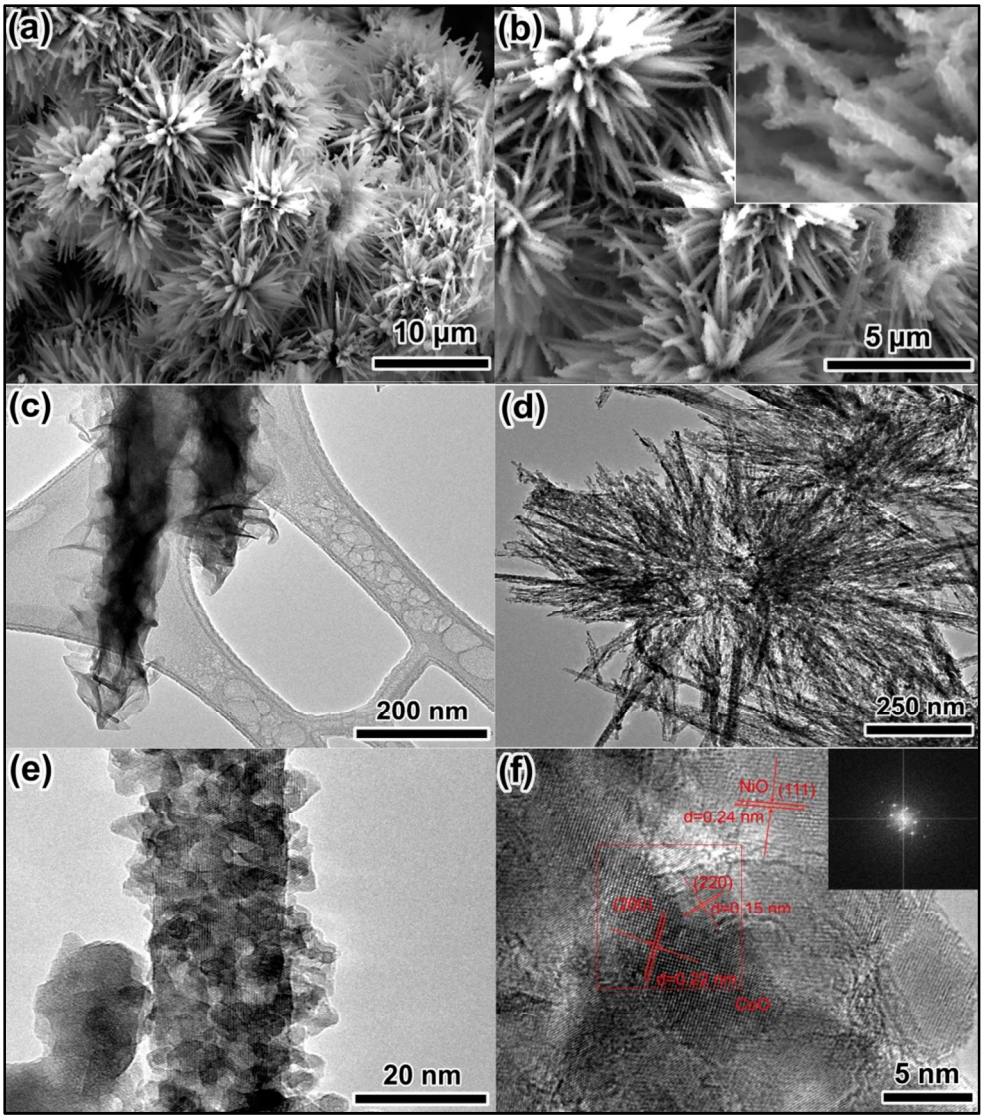

Figure 3 (a-b) SEM images of core/shell CoO@NiO nanostructure on ACT fibers at different magnifications; (c) TEM image of core/shell CoO@NiO precursor; (d-f) TEM and HRTEM images of core/shell CoO@NiO nanostructure, inset of f is the corresponding FFT pattern.

Ordered 1D CoO nanowires are thought to possess good electrochemical properties because they have easier electron transport paths and larger active interfacial sites. Therefore, urchin-like CoO nanosphere architecture was chosen as a backbone (core) to deposit a layer of NiO nanoflakes (shell). Figures 3a-b show the morphology of the as-prepared urchin-like CoO@NiO core/shell nanostructure on ACT fibers. The CoO nanowires have an average diameter of ~70 nm, and the length up to ~5 μm. After the chemical bath deposition, uniform NiO nanoflakes were grown on the entire framework, forming a conformal NiO coating on the surface of CoO nanowires. The interconnected

NiO nanoflake shells with a thickness of ~30 nm were uniformly decorated on the CoO backbone. The TEM images (Figures 3c-d) clearly reveal the details of such core/shell CoO@NiO nanostructure. After the heat treatment, mesopores with the size of 2-4 nm appeared on the CoO nanowires (Figure 3e), which are anticipated to exhibit high electrochemical properties due to the high density of active sites and short electron transport path. The tiny NiO nano-flakes decorated on CoO nanowires render highly porous hierarchical nanostructure, which serves as a reservoir for electrolyte ions, providing dense diffusion channels for ion transport. Figure 3f shows the HRTEM image and corresponding FFT pattern of the core/shell CoO@NiO nanostructure. A clear grain boundary between the core and shell is apparent, with the interplanar spacings of 0.22 nm and 0.15 nm for the cubic phase CoO core, and 0.28 nm for the NiO shell, respectively.

Figure S1 shows the typical XRD patterns of the obtained sheet-like, petal-like, urchin-like CoO/ACT and the hierarchical core/shell CoO@NiO/ACT composite. The diffraction peaks of sheet-like CoO/ACT, petal-like CoO/ACT, urchin-like CoO/ACT can be indexed to the (111), (200), and (220) planes of the cubic CoO phase (JCPDS card no. 44-0962). Interestingly, not only the morphologies of the obtained CoO nano-architectures changed, but also the crystallinity increased with increasing reactant concentration. The deposition of NiO shell on the urchin-like CoO/ACT significantly enhanced the diffraction intensity. However, it is difficult to differentiate the feature diffraction peaks among CoO and NiO (JCPDS card no. 65-2901), due to the similarity of their cubic crystal structures.

3.2 Negative Electrode Materials

Graphene has been regarded as a promising electrode material for energy storage and conversion due to its high surface area and superior conductivity. To further exploit its potential for flexible electrode, graphene-based films/papers and 3D porous graphene structures have been widely used to overcome the restacking and aggregation of graphene nanosheets. In this study, a flexible ACT coated with graphene nanosheets was used as the negative electrode to construct asymmetric supercapacitors.

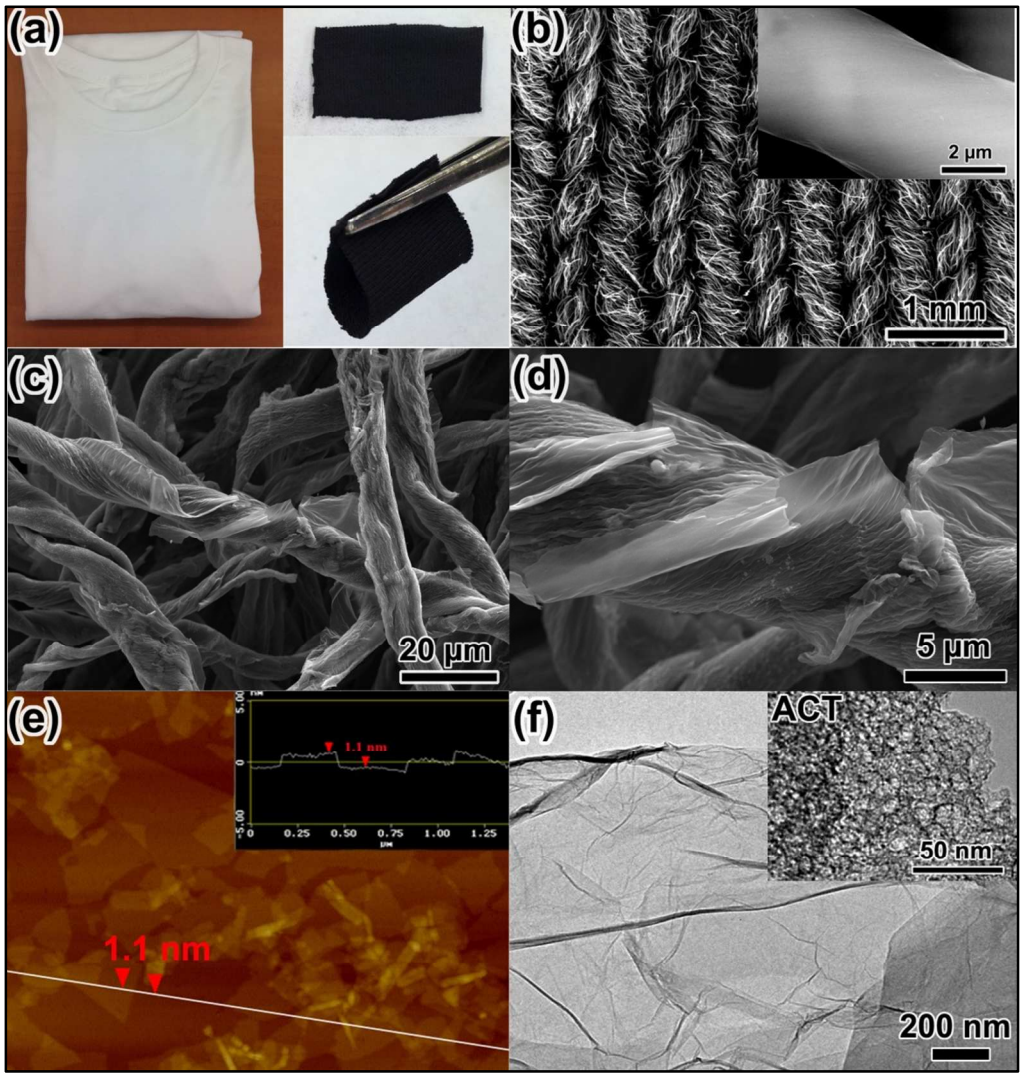

Figure 4 (a) Optical photographs of a cotton T-shirt, insets are a piece of ACT and a piece of ACT under folding state, showing its high flexibility; (b) SEM image of ACT, inset is the amplified SEM image; (c and d) SEM images of ACT coated with graphene sheets; (e) AFM image of graphene oxide with highlighted profile; (f) TEM image of graphene oxide nanosheet, inset is the TEM image of ACT.

Negative ACT/graphene electrode material was obtained by dipping ACT in a graphene oxide solution. ACT was prepared by direct conversion of a cotton T-shirt, as shown in Figure 4a. After activation, ACT was mechanically flexible even under folding state (inset of Figure 4a) and highly conductive (surface resistance: ~10-20 ohm/sq). Figure 4b is the SEM image of a piece of activated cotton textile, showing that the interwoven fibers of ACT inherit the cellulose fiber structure of cotton textile with the diameters ranging from 5 to 10 μm (inset of Figure 4b). After dipping ACT in the graphene oxide solution, individual ACT fibers were wrapped with single layered, curled

and entangled graphene oxide sheet with a thickness of ~1.1 nm (Figures 4e and f). In the reduction process, reduced graphene oxide sheets were restored and conjugated, inducing partial overlapping or coalescing via π-π stacking or hydrogen bonding[54,55] and consequently resulting in an interconnected 3D network (Figures 4c and d). Interestingly, the ACT fibers also showed porous structure, as revealed by TEM image (the inset of Figure 4f). The coalesced and twisted graphene nanosheets randomly wrapped porous ACT fibers, forming a porous conductive ACT/graphene composite which serves as electron "highway" and collector. Such well-defined 3D porous structure is anticipated to facilitate electrolyte ion diffusion and electron transport in the rapid charge/discharge process, which in turn will improve the overall energy density of the cell.

Figure 5a shows the XRD patterns of cotton textile, ACT, ACT/graphene oxide and ACT/graphene. After activation, cotton's (101), (002) and (040) peaks[56] disappeared, instead ACT exhibited a broader diffraction peak around 21°, pointing toward amorphous carbon. The ACT/graphene oxide exhibited a peak at 8.8°, corresponding to the (001) lattice plane of graphene oxide with a d-spacing of 0.78 nm. This indicates that graphite was completely exfoliated to single layered graphite oxide.[57] The peak at 8.8° disappeared for the ACT/graphene, indicating the complete reduction of graphene oxide to graphene.[58,59] Raman spectroscopy is an important nondestructive tool for characterizing graphitic materials, especially the ordered and disordered crystal structures of graphene.[60] The Raman spectrum of graphene usually can be characterized by two main feature bands: the G band arising from the first order scattering of the E1g phonon of sp2 C atoms at about 1575 cm^{-1} and the D band arising from a breathing mode of point photons of A1g symmetry at about 1350 cm^{-1}.[61] Compared with ACT/graphite oxide, an increased I_D/I_G ratio of the ACT/graphene was observed (Figure 5b), indicating that the oxygen functional groups in graphene oxide sheets were removed and the conjugated graphene network (sp^2 carbon) was also reestablished during the heat reduction process.[62] The increase in the intensity ratio (I_D/I_G) is believed to result from the reestablishment of graphene network during the annealing process, suggesting a relative smaller average size and more defects and disordered structures than that of the original graphite oxide.[63,64]

The results jointly demonstrate that most of the oxygen-containing groups have been successfully removed during the heat reduction process, which is consistent with the XRD data.

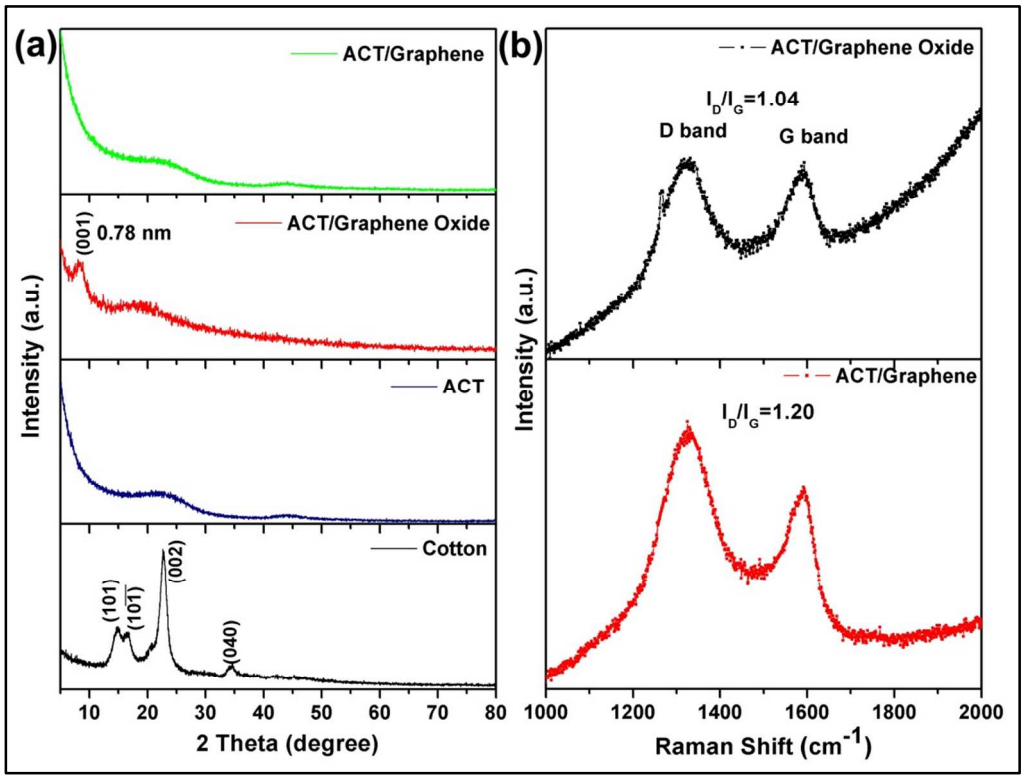

Figure 5 (a) Typical XRD patterns of cotton textile, ACT, ACT/graphene oxide and ACT/graphene; (b) Raman spectra of ACT/graphene oxide, and ACT/graphene.

3.3 Electrochemical Performance

A flexible asymmetric supercapacitor was constructed by two electrodes (1 × 2 cm^2) cemented with the PVA-KOH gel serving as both the solid electrolyte and separator, as schematically illustrated in Figure 6a. The as-prepared CoO/ACT with different morphologies and the hierarchical core/shell CoO@NiO/ACT were used as positive electrodes, whereas ACT/graphene was used as the negative electrode. The electrochemical performances of the asymmetric supercapacitors were investigated by cyclic voltammetry (CV) and galvanostatic charge/discharge and electrochemical impedance spectra (EIS) measurements under a two-electrode system.

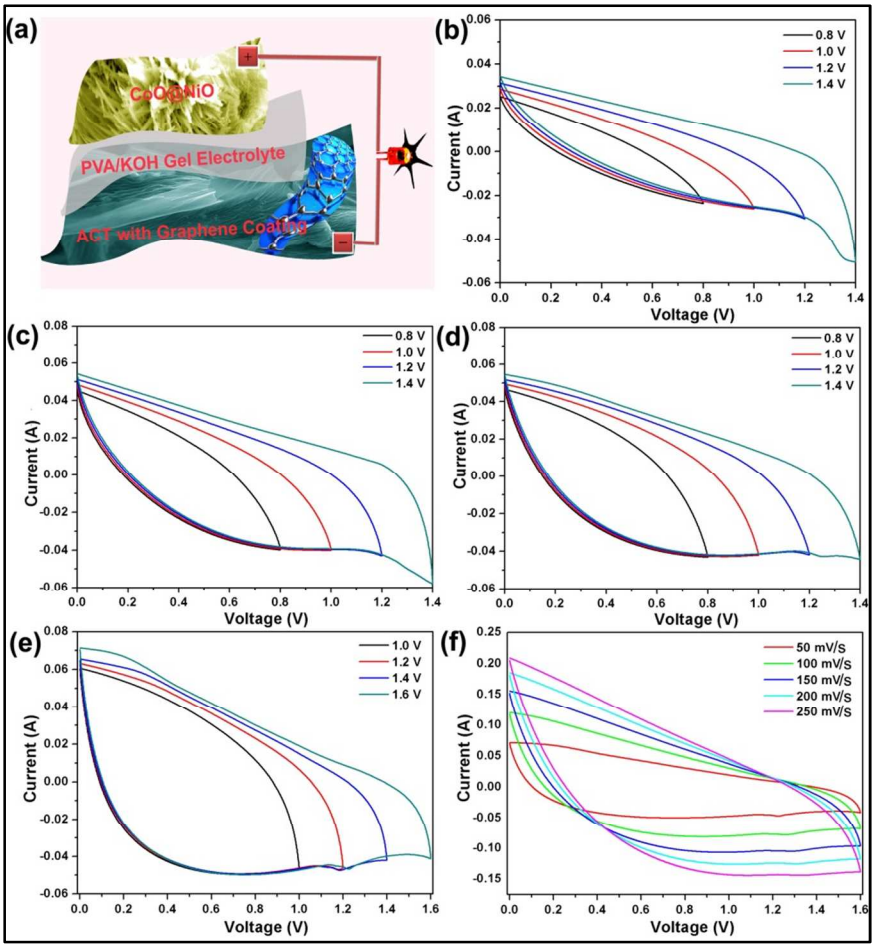

Figure 6 (a) Illustration of the assembled flexible all-solid-state asymmetric supercapacitor; (b) CV curves of sheet-like CoO/ACT//ACT/graphene asymmetric supercapacitor with PVA/KOH polymer gel electrolyte under the voltage windows of 0.8, 1.0, 1.2 and 1.4 V at the scan rate of 50 mV s^{-1}; (c) CV curves of petal-like CoO//ACT/graphene asymmetric supercapacitor with PVA/KOH polymer gel electrolyte under the voltage windows of 0.8, 1.0, 1.2 and 1.4 V at the scan rate of 50 mV s^{-1}; (d) CV curves of urchin-like CoO//ACT/graphene asymmetric supercapacitor with PVA/KOH polymer gel electrolyte under the voltage windows of 0.8, 1.0, 1.2 and 1.4 V at the scan rate of 50 mV s^{-1}; (e) CV curves of core/shell CoO@NiO//ACT/graphene asymmetric supercapacitor with PVA/KOH polymer gel electrolyte under the voltage windows of 1, 1.2, 1.4 and 1.6 V at the scan rate of 50 mV s^{-1}; (b) CV curves of core/shell CoO@NiO//ACT/graphene asymmetric supercapacitor with PVA/KOH polymer gel electrolyte under the voltage windows of 1.6 V at different scan rates.

Figures 6b-d show the CV curves of CoO/ACT//ACT/graphene asymmetric supercapacitors with the PVA/KOH polymer gel electrolyte under the voltage windows of 0.8, 1.0, 1.2 and 1.4 V at the scan rate of 50 mV s^{-1}. It can be seen that the working voltage for those CoO/ACT//ACT/graphene asymmetric supercapacitors can be extended to 1.4 V, which is essential for practical application. Compared with the sheet-like CoO/ACT cell, the CV curves for the petal-like and urchin-like CoO/ACT cells showed

better rectangularity, suggesting lower charge transfer resistance and better rate performance. Although the shape of CV curves for the petal-like CoO/ACT cell and urchin-like CoO/ACT cell are similar, the integrated area based on the CV curve of the urchin-like petal-like CoO/ACT cell is larger than that of the petal-like CoO/ACT cell at different potential windows, indicating a higher capacitance for the urchin-like CoO/ACT cell. Therefore, the urchin-like CoO/ACT nanowire was further selected for the fabrication of hierarchical porous core/shell CoO@NiO/ACT composite electrode for high performance flexible supercapacitors. Figure 6e shows the CV curves of the flexible all-solid-state core/shell CoO@NiO/ACT//ACT/graphene asymmetric supercapacitor at the different voltage windows, performed at the scan rate of 50 mV s^{-1}. Compared with the CoO/ACT cells with different CoO nanostructures, the fabricated core/shell CoO@NiO/ACT//ACT/graphene asymmetric cell showed combined pseudo-capacitive and electric double-layer capacitive behaviors, even at a high working potential up to 1.6 V. Therefore, the operation potential window was chosen as 1.6 V for the core/shell CoO@NiO/ACT to further evaluate its supercapacitor performance. Figure 6f shows the CV curves of the CoO@NiO/ACT//ACT/graphene asymmetric cell at different scan rates ranging from 50 to 250 mV s^{-1} at the operation window of 1.6 V. Apparently, all the curves exhibit a similar shape, and the current density increases with increasing scan rate, indicating stable reversibility and excellent rate performance.

The charge storage is ascribed to the Faradaic redox reactions of CoO and NiO in the PVA-KOH electrolyte as follows: [65,66]

$$4CoO + 4OH^- \rightarrow 2H_2O + 2Co_2O_3 + 4e^- \quad (8)$$

$$NiO + OH^- \rightarrow NiOOH + e^- \quad (9)$$

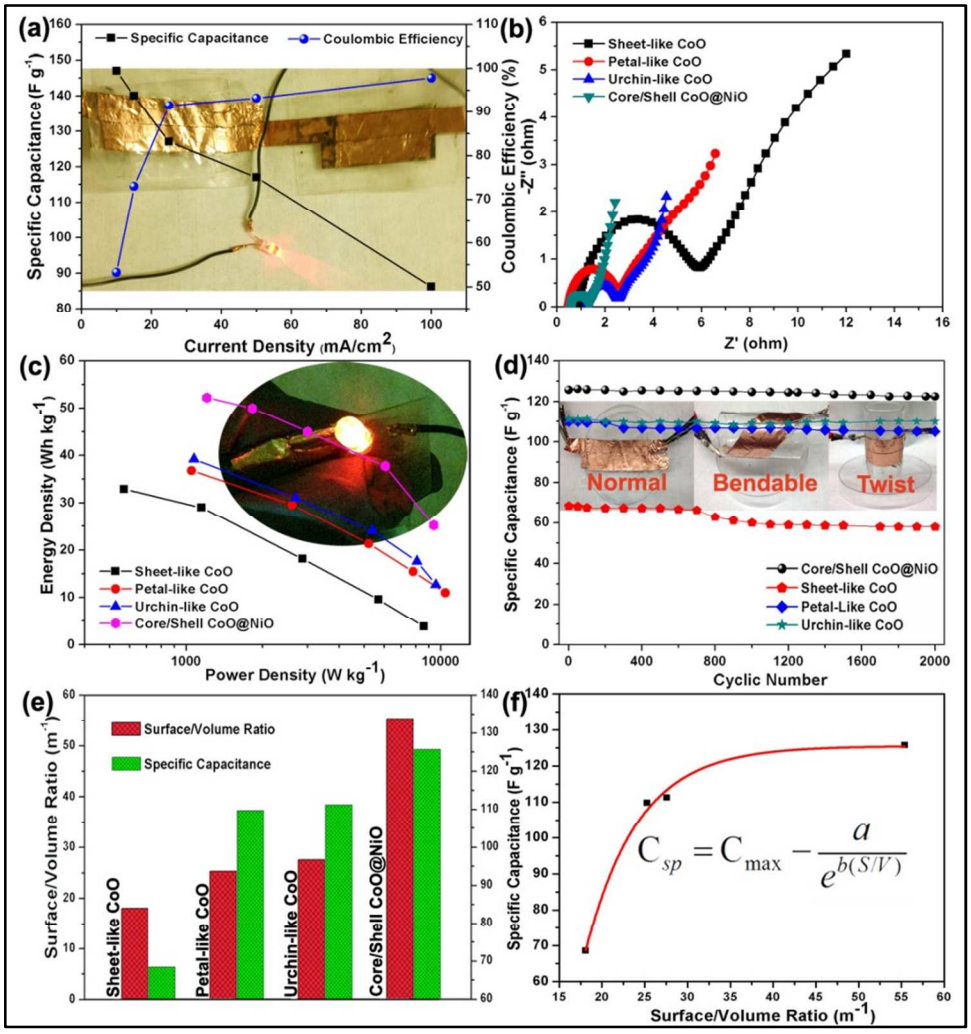

Figure 7 (a) Specific capacitances and Coulombic efficiency of the core/shell CoO@NiO/ACT//ACT/graphene asymmetric supercapacitor with PVA/KOH as polymer gel electrolyte, inset shows a lighted LED by two asymmetric supercapacitors connected in series; (b) Nyquist plots of the sheet-like CoO/ACT//ACT/graphene supercapacitor, petal-like CoO/ACT//ACT/graphene, urchin-like CoO/ACT//ACT/graphene and core/shell CoO@NiO/ACT//ACT/graphene asymmetric supercapacitors with PVA/KOH polymer gel electrolyte; (c) Ragone plots of the as-assembled sheet-like CoO/ACT//ACT/graphene supercapacitor, petal-like CoO/ACT//ACT/graphene, urchin-like CoO/ACT//ACT/graphene and core/shell CoO@NiO/ACT//ACT/graphene asymmetric supercapacitors with PVA/KOH polymer gel electrolyte, inset shows the lighted LED by the asymmetric supercapacitor even under totally folded state; (d) Cyclic performance of the sheet-like CoO/ACT//ACT/graphene supercapacitor, petal-like CoO/ACT//ACT/graphene, urchin-like CoO/ACT//ACT/graphene and core/shell CoO@NiO/ACT//ACT/graphene asymmetric supercapacitors with PVA/KOH polymer gel electrolyte under different working condition; (e) Surface/volume ratios and specific capacitances of sheet-like CoO , petal-like CoO , urchin-like CoO and the as-prepared hierarchical core/shell CoO@NiO nanocomposite; (f) Fitting result and corresponding mathematical expression of the relationship between surface/volume ratio and specific capacitance.

However, unlike traditional pseudo-capacitive electrode, the CoO@NiO/ACT//ACT/graphene asymmetric cell displayed a quasi-rectangular CV geometry, indicating an electrochemical double layer capacitor behavior.

Figure S2 shows the typical galvanostatic charging/discharging curves of the different morphological CoO/ACT//ACT/graphene and core/shell CoO@NiO/ACT//ACT/graphene asymmetric supercapacitors at different current densities. The cell voltage of the as-fabricated CoO/ACT is 1.4 V, while the cell voltage can be expanded to 1.6 V (from 0 to 1.6 V) for the core/shell CoO@NiO/ACT//ACT/graphene asymmetric cell without showing obvious IR drop, which could be attributed to the small internal resistance. The specific capacitances for the sheet-like CoO@NiO/ACT, petal-like CoO@NiO/ACT, urchin-like CoO@NiO/ACT and core/shell CoO@NiO/ACT asymmetric cells at the current density of 10 mA cm^{-2} are 106, 135, 138, and 147.6 F g^{-1}, respectively. The large specific capacitance, symmetric charging/discharging curves and good linear relationship could be ascribed to the synergistic effects of the hierarchical CoO@NiO nanostructure and the electrochemical double layer capacitance of ACT/graphene, indicating excellent electrochemical capacitive characteristic and superior reversible redox reaction.

Rate performance and coulombic efficiency are also important factors for real power application. To further evaluate the potential of the core/shell CoO@NiO/ACT//ACT/graphene asymmetric cell for practical application, the galvanostatic charge/discharge tests were carried out at different current densities ranging from 10 to 100 mA cm^{-2} (Figure 7a). The corresponding specific capacitances for the asymmetric supercapacitor are respectively 147.6 F g^{-1} at 10 mA cm^{-2} and 86.7 F g^{-1} at 100 mA cm^{-2} with a capacitance retention of 58.7% while the current density was increased by 10 times, suggesting great rate performance for the asymmetric CoO@NiO/ACT//ACT/graphene supercapacitor. The coulombic efficiency exhibited a fast increase at the initial stage from 53.3% at 10 mA cm^{-2} to 91.52 at 25 mA cm^{-2} and then a gradual increase up to 98.8%. The high coulombic efficiency is very important for enhancing the energy utilization efficiency and promoting electrochemical reversibility,

which can be ascribed to the hierarchal structure with higher activated surface, improved mass transportation, and good conductivity.

Electrochemical impedance spectroscopy (EIS) is one of the principal methods for studying the fundamental electrochemical behavior of supercapacitors. For an in-depth understanding of the electrochemical mechanism in the all-solid-state asymmetric supercapacitors, the impedance spectra of CoO@NiO/ACT//ACT/graphene with different morphologies and core/shell CoO@NiO/ACT//ACT/graphene asymmetric supercapacitors were measured in the frequencies ranging from 100 kHz to 0.05 Hz at the open circuit potential with an AC perturbation of 5 mV. All the impedance spectra exhibit a similar shape, with an arc at high frequency and a straight line at low frequency (Figure 7b). The high-frequency arc corresponds to the charge transfer limiting process, which is ascribed to the double-layer capacitance (C_{dl}) and the charge transfer resistance (R_{ct}) at the interface between electrode and electrolyte solution.[67] The charge-transfer resistance R_{ct} was directly measured from the diameter of the semicircle arc. Compared with the R_{ct} of CoO/ACT//ACT/graphene cells with different morphologies (sheet-like CoO/ACT (4.91 Ω), petal-like CoO/ACT (2.05 Ω), urchin-like CoO/ACT (1.37 Ω)), the core/shell CoO@NiO/ACT//ACT/graphene displays the smallest R_{ct} (0.81 Ω), indicating the good electron transport path and easy ions accessibility for the core/shell CoO@NiO/ACT//ACT/graphene cell. In addition, the straight line at low frequency exhibits a slope closer to 90°, indicating the improved conductivity and low ions diffusion resistance for core/shell CoO@NiO/ACT//ACT/graphene cell.[68]

Energy density and power density are also important factors for evaluating the practical application potentials of supercapacitors. It is expected that the good supercapacitor could provide both high energy density and high power density at high charge/discharge rates. Figure 7c shows the Ragone plots of all-solid-state flexible CoO/ACT//ACT/graphene and core/shell CoO@NiO/ACT//ACT/graphene asymmetric cells. All the asymmetric cells showed a similar trend of energy density and power density. Compared with the CoO/ACT//ACT/graphene cells, encouragingly, the core/shell CoO@NiO/ACT//ACT/graphene asymmetric cell achieved a higher energy

density of 52.26 Wh kg^{-1} at the power density of 1206 W kg^{-1}, and remained 25.2 Wh kg^{-1} at the power density of 9.53 KW kg^{-1}. The superior performances for the core/shell CoO@NiO/ACT//ACT/graphene asymmetric cell are ascribed to the synergistic effects of ACT/graphene and hierarchical core/shell CoO@NiO nanostructure.

A long cycling performance is another crucial requirement for the practical application of supercapacitors. Figure 7d shows the cyclic performances of the flexible all-solid-state CoO/ACT//ACT/graphene and core/shell CoO@NiO/ACT//ACT/graphene asymmetric cells, examined by galvanostatic charge/discharge tests at the constant current density of 25 mA cm^{-2} t under different mechanical states (normal, bent and twisted states) for up to 2000 cycles. All the asymmetric cells exhibit small capacitance decay during the cyclic tests. Encouragingly, the core/shell CoO@NiO/ACT//ACT/graphene asymmetric cell showed an increase in specific capacitance at the initial 50 cycles under normal state, which is ascribed to the complete exposure and full use of Ni and Co active sites. It is remarkable that 97.53% of its pristine specific capacitance was maintained after 2000 cycles, even at the bent and twisted states (inset of Figure 7d), indicating excellent mechanical flexibility, electrochemical robustness and cycle stability. The digital photographs of the as-assembled flexible supercapacitors packed with PET tape are shown in the inset of Figure 7a to demonstrate its practical application. Two as-assembled flexible all-solid-state cells were then connected in series to light a commercial red LED (inset of Figure 7a). Even in a folded state (inset of Figure 7c), the brightness of the lightened LED did not change, showing its excellent coupled mechanical and electrochemical robustness. All in all, the core/shell CoO@NiO/ACT//ACT/graphene asymmetric cell exhibited superior electrochemical stability, which is believed to result from the unique structure of the CoO@NiO nanostructure and graphene, the intimate interfacial contact between hierarchal core/shell CoO@NiO and ACT substrate, high electrical conductivity of the wrapped graphene, and the excellent mechanical robustness of both electrodes and gel electrolyte film.

Based on the above electrochemical analysis, it can be seen that the electrochemical properties of CoO nanostructures are strongly morphology-dependent. To unveil the

relationship between the morphology and electrochemical performance, 3D morphology models were established by using Autodesk 3ds Max for individual nano-architectures to estimate their surface/volume ratios, according to their size from the SEM images (Figures 2 and 3). Figure 7e shows the surface/volume ratios and specific capacitances of the prepared CoO nanostructures with different morphologies and the core/shell CoO@NiO composite. It can be seen that the architecture with a larger surface area exhibits higher specific capacitance. The relationship between the specific capacitance and surface/volume ratio can be well fitted by a negative exponential function (Figure 7f):

$$C_{sp} = C_{\max} - \frac{a}{e^{b(S/V)}} \quad (10)$$

where C_{sp} is the specific capacitance, C_{max} is the theoretical specific value for the system with the specific positive electrode, negative electrode and electrolyte, S/V is the surface/volume ratio, *a and* b are constants which are system dependent. Here, the theoretical maximum specific capacitance (C_{max}) of the assembled cell at the current density of 25 mA cm^{-2} *is* 125.47756 F g^{-1}, the constants *a* and *b* are 1084.2981 and 0.1829, respectively. Clearly, the hierarchical core/shell CoO@NiO composite possesses higher surface/volume ratio and higher specific capacitance than other CoO nano-architectures. Thus, specific surface area plays an import role in specific capacitance. However, there exists an upper limit (C_{max}), which cannot be exceeded. Upon approaching to the upper limit, further increasing specific surface area cannot push up specific capacitance much. This finding provides an important guideline for electrode materials design, microstructure control and system construction.

4. Conclusion

Battery-type faradic CoO nanoarchitectures with different morphologies (sheet-like, petal-like and urchin-like) were controllably synthesized on ACTs by simply changing the reactant concentration during the hydrothermal process. The electrochemical properties of CoO nanostructures were found to be strongly morphology-dependent. The specific capacitance increased exponentially with the surface/volume ratio of

nanostructures. Due to its higher surface/volume ratio and better electrochemical performance, the urchin-like CoO nanowire was further chosen as the backbones (core) for depositing a layer of pseudocapacitive NiO nano-flakes (shell) to construct a hierarchical 3D porous core/shell CoO@NiO/ACT nanostructure with super surface, which is beneficial for the charge accumulation and ion transport, enabling the high performance for flexible supercapacitor application. In addition, the activation of cotton textiles into porous, highly conductive ACTs with high accessible surface area, and the good electrical conductivity rendered by wrapped graphene, endowed the flexible asymmetric supercapacitor with higher rate performance. PVA-KOH solid-state gel was used as both the electrolyte and separator. Finally, the assembled CoO@NiO/ACT//ACT/graphene asymmetric supercapacitor exhibited an exceptional combination of mechanical and electrochemical performances, including high specific capacitance, remarkable energy density and power density, exceptional high operating potential (1.6 V), excellent cycling stability and eminent mechanial roubustness. This work opens up unprecedented opportunities for designing hybrid transition metal oxides and graphene on flexible ACTs nanoarchitectures for next generation flexible/wearable energy storage devices.

Acknowledgements

Financial support for this study was provided by the U.S. National Science Foundation (CMMI-1418696 and CMMI-1358673) and the i6 Virginia Innovation Partnership. The authors thank the staff members at the University of Virginia NMCF for electron microscopy technical support.

References

(1) J. M. Tarascon, *Philos. Trans. A. Math. Phys. Eng. Sci.* 2010, ***368***, 3227.

(2) P. Simon and Y. Gogotsi, *Nat. Mater.* 2008, ***7***, 845.

(3) B. E. Conway, Electrochemical Supercapacitors: Scientic Fundamentals and Technological Applications, Kluwer Academic Publishers/Plenum Press, New York, 1999.

(4) A. Burke, *J. Power Sources* 2000, ***91***, 37.

(5) M. S. Halper and J. C. Ellenbogen, *Supercapacitors: a Brief Overview*, MITRE Nanosystems Group, Virginia, 2006

(6) G. Yu, L. Hu, N. Liu, H. Wang, M. Vosgueritchian, Y. Yang, Y. Cui and Z. Bao, *Nano Lett.* 2011, ***11***, 4438.

(7) L. Bao, J. Zang and X. Li, *Nano Lett.* 2011, ***11***, 1215.

(8) J. W. Jeon, R. Sharma, P. Meduri, B. W. Arey, H. T. Schaef, J. L. Lutkenhaus, J. P. Lemmon, P. K. Thallapally, M. I. Nandasiri, B. P. McGrail and S. K. Nune, *ACS Appl. Mater. Interfaces* 2014, ***6***, 7214.

(9) E. Frackowiak, Carbon Materials for Supercapacitor Application. *Phys. Chem. Chem. Phys.* 2007, ***9***, 1774.

(10) Y. B. Tan and J. M. Lee, *J. Mater. Chem. A* 2013, ***1***, 14814.

(11) H. Pan, J. Li and Y. P. Feng, *Nanoscale Res. Lett.*, 2010, ***5***, 654.

(12) Q. Liang, L. Ye, Z. H. Huang, Q. Xu, Y. Bai, F. Kang and Q. H. Yang, *Nanoscale* 2014, ***6***, 13831.

(13) C. C. Hu, K. H. Chang, M. C. Lin and Y. T. Wu, *Nano Lett.* 2006, ***6***, 2690.

(14) P. Yu, X. Zhang, D. Wang, L. Wang and Y. Ma, *Cryst. Growth Des.* 2009, ***9***, 528.

(15) W. Yang, Z. Gao, J. Ma, J. Wang, B. Wang and L. Liu, *Electrochim. Acta* 2013, ***112***, 378.

(16) J. Li, W. Zhao, F. Huang, A. Manivannan and N. Wu, *Nanoscale* 2011, ***3***, 5103.

(17) Z. Gao, W. Yang, Y. Yan, J. Wang, J. Ma, X. Zhang, B. Xing and L. Liu, *Eur. J. Inorg. Chem.* 2013, **27**, 4832.

(18) G. A. Snook, P. Kao and A. S. Best, *J. Power Sources* 2011, ***196***, 1.

(19) K. Jurewicz, S. Delpeux, V. Bertagna, F. Béguin and E. Frackowiak, *Chem. Phys. Lett.* 2001, ***347***, 36.

(20) W. Yang, Z. Gao, N. Song, Y. Zhang, Y. Yang and J. Wang, *J. Power Sources* 2014, ***272***, 915.

(21) H. Wei, Y. Wang, J. Guo, X. Yan, R. O'Connor, X. Zhang, N. Z. Shen, B. L. Weeks, X. Huang, S. Wei and Z. Guo, ChemElectroChem, 2015, 2, 119-126.

(22) C. Liu, F. Li, L. P. Ma and H. M. Cheng, *Adv. Mater.* 2010, ***22***, E28.

(23) R. B. Rakhi, W. Chen, D. Cha and H. N. Alshareef, *Mater. Renew. Sustain. Energy* 2013, ***2***, 17.

(24) H. Wang, Z. Xu, H. Yi, H. Wei, Z. Guo and X. Wang, Nano Energy, 2014, 7, 86-96.

(25) K. Jost, G. Dion and Y. Gogotsi, *J. Mater. Chem. A* 2014, ***2***, 10776.

(26) W. Yang, Z. Gao, J. Ma, X. Zhang, J. Wang and J. Liu, *J. Mater. Chem. A* 2014, ***2***, 1448.

(27) L. Yuan, X. Lu, X. Xiao, T. Zhai, J. Dai, F. Zhang, B. Hu, X. Wang, L. Gong, J. Chen, C. Hu, Y. Tong, J. Zhou and Z. L. Wang, *ACS Nano*, 2012, ***6***, 656.

(28) C. Meng, C. Liu, L. Chen, C. Hu and S. Fan, *Nano Lett.* 2010, ***10***, 4025.

(29) C. D. Lokhande, D. P. Dubal and O. S. Joo, *Curr. Appl. Phys.* 2011, ***11***, 255.

(30) P. Simon, Y. Gogotsi and B. Dunn, *Science*, 2014, ***343***, 1210.

(31) X. Xia, J. Tu, Y. Zhang, X. Wang, C. Gu, X. B. Zhao and H. J. Fan, *ACS Nano* 2012, ***6***, 5531.

(32) G. Zhang, T. Wang, X. Yu, H. Zhang, H. Duan and B. Lu, *Nano Energy* 2013, ***2***, 586.

(33) Z. Gao, N. N. Song, Y. Y. Zhang and X. D. Li, *RSC Adv.* 2015, ***5***, 15438.

(34) P. Liu, Z. Hu, Y. Liu, M. Yao, Q. Zhang and Z. Xu, *Int. J. Electrochem. Sci.* 2014, ***9***, 7986.

(35) D. Lan, Y. Chen, P. Chen, X. Chen, X. Wu, X. Pu, Y. Zeng and Z. Zhu, *ACS Appl. Mater. Interfaces* 2014, ***6***, 11839.

(36) C. Zhou, Y. Zhang, Y. Li, J. Liu, C. Zhou, Y. Zhang, Y. Li. And J. Liu, *Nano Lett*. 2013, **13**, 2078.

(37) C. Guan, X. Li, Z. Wang, X. Cao, C. Soci, H. Zhang and H. J. Fan, *Adv. Mater.* 2012, ***24***, 4186.

(38) Z. Fan, J. Yan, T. Wei, L. Zhi, G. Ning, T. Li and F. Wei, *Adv. Funct. Mater.* 2011, ***21***, 2366.

(39) Y. G. Wang, Z. D. Wang and Y. Y. Xia, *Electrochim. Acta* 2005, ***50***, 5641.

(40) Y. B. Tan and J. M. Lee, *J. Mater. Chem. A* 2013, ***1***, 14814.

(41) J. Liu, L. Zhang, H. B. Wu, J. Lin, Z. Shen and X. W. (David), Lou, *Energy Environ. Sci.* 2014, ***7***, 3709.

(42) H. Gao, F. Xiao, C. B. Ching and H. Duan, *ACS Appl. Mater. Interfaces* 2012, ***4***, 2801.

(43) A. Sumboja, C. Y. Foo, X. Wang and P. S. Lee, *Adv. Mater.* 2013, ***25***, 2809.

(44) Z. Gao, W. Yang, J. Wang, N. Song and X. Li, *Nano Energy* 2015, ***13***, 306.

(45) A. G. Avila and J. P. Hinestroza, *Nat. Nanotechnol.* 2008, ***3***, 458-459.

(46) L. Bao, and X. Li, *Adv. Mater.* 2012, ***24***, 3246.

(47) X. H. Xia, J. P. Tu, J. Zhang, X. L. Wang, W. K. Zhang and H. Huang, *Sol. Energy Mater. Sol. Cells* 2008, ***92***, 628.

(48) W. S. Hummers and R. E. Offeman, *J. Am. Chem. Soc.* 1958, ***80***, 1339-1339.

(49) G. Li, W. Li, K. Xu, R. Zou, Z. Chen and J. Hu, *J. Mater. Chem. A* 2014, ***2***, 7738.

(50) Y. G. Zhu, Y. Wang, Y. Shi, J. I. Wong and H. Y. Yang, *Nano Energy* 2014, ***3***, 46.

(51) K. Cao, L. Jiao, Y. Liu, H. Liu, Y. Wang and H. Yuan, *Adv. Funct. Mater.* 2015, ***25***, 1082.

(52) W. P. Zhang, B. G. Zhao, C. D. Zou, Q. J. Zhai and Y. L. Gao, *Trans. Nonferrous Met. Soc. China English Ed.* 2013, ***23***, 1668.

(53) P. W. Voorhees, *J. Statist. Phys* 1985, ***38***, 231..

(54) H. Bai, C. Li, X. Wang and G. Shi, *J. Phys. Chem. C* 2011, ***115***, 5545.

(55) W. Chen and L. Yan, *Nanoscale* 2011, ***3***, 3132.

(56) E. N. J. Ford, S. K. Mendon, S. F. Thames and J. W. Rawlins, *J. Eng. Fiber. Fabr.* 2010, ***5***, 10.

(57) Z. H. Liu, Z. M. Wang, X. Yang and K. Ooi, *Langmuir* 2002, ***18***, 4926.

(58) H. M. A. Hassan, V. Abdelsayed, A. E. R. S. Khder, K. M. AbouZeid, J. Terner, M. S. El-Shall, S. I. Al-Resayes and A. A. El-Azhary, *J. Mater. Chem.* 2009, ***19***, 3832.

(59) M. J. McAllister, J. L. Li, D. H. Adamson, H. C. Schniepp, A. A. Abdala, J. Liu, M. Herrera-Alonso, D. L. Milius, R. Car, R. K. Prud'homme and I. A. Aksay, *Chem. Mater.* 2007, ***19***, 4396.

(60) G. Bronoel, A. Millot and N. Tassin, *J. Power Sources* 1991, ***34***, 243.

(61) A. Ferrari and J. Robertson, *Phys. Rev. B* 2000, ***61***, 14095.

(62) Z. Ji, X. Shen, M. Li, H. Zhou, G. Zhu and K. Chen, *Nanotechnology* 2013, ***24***, 115603.

(63) C. Xu, X. Wang and J. Zhu, *J. Phys. Chem. C* 2008, **112**, 19841.

(64) Y. Wang, Q. He, H. Qu, X. Zhang, J. Guo, J. Zhu, G. Zhao, H. A. Colorado, J. Yu, L. Sun, S. Bhana, M. A. Khan, X. Huang, D. P. Young, H. Wang, X. Wang, S. Wei and Z. Guo, J. Mater. Chem. C, 2014, 2, 9478-9488.

(65) C. Zheng, C. Cao, Z. Ali and J. Hou, *J. Mater. Chem. A* 2014, ***2***, 16467.

(66) K. Liang, X. Tang and W. Hu, *J. Mater. Chem.* 2012, ***22***, 11062.

(67) A. D. Fabio, A. Giorgi, M. Mastragostino and F. Soavi, *J. Electrochem. Soc.* 2001,***148***, A845.

(68) G. J. Brug, A. V. Eeden, M. Sluyters-Rehbach and J. H. Sluyters, *J. Electroanal. Chem.* 1984, ***176***, 275.

Graphic Abstract

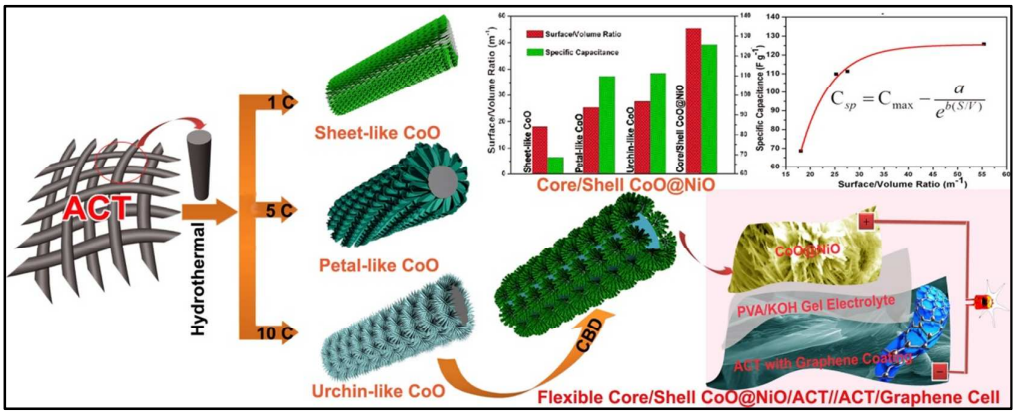

Table of Contents:

Core/Shell CoO@NiO//ACT/Graphene asymmetric cell was assembled with unique nanostructures for high performance flexible supercapacitor.